Chapter 2

Plasmonic response of nanoparticles under Plane wave illumination

This chapter introduces the Mie Scattering Algorithm developed on the MATLAB platform to examine the interaction of a linearly polarized plane wave with a nanoparticle. A theoretical formulation for intensity enhancement in near-field due to the plasmonic response of nanoparticles is presented. Radial and tangential components of average intensity enhancement are discussed and results are shown for varying radius sizes of monometallic and core-shell nanoparticles.

2.1 Introduction: Mie Scattering Theory

Scattering by small particles of size comparable to the incident light wavelength is an important topic in a wide variety of scientific and technical fields. Mie theory has been extensively used to examine scattering by a single homogeneous sphere made up of any arbitrary material [59, 65, 108, 109, 128]. Mie theory provides critical insights into how light interacts with spherical particles, offering applied benefits across diverse fields. In atmospheric science, it helps to model how aerosols and water droplets scatter light, aiding climate studies and weather prediction [120]. In biomedical optics, it enables the characterization of cells and nanoparticles for diagnostic imaging and therapies [121, 129, 130]. Additionally, remote sensing utilizes Mie theory to analyze atmospheric particles, while industrial processes use it for particle sizing and quality control in aerosols and suspensions [131]. The importance of Mie theory has interestingly increased in nanotechnology, especially in plasmonics. Mie theory, in particular, offers a framework for comprehending the optical characteristics of a metallic nanoparticle, which include LSPR.

Using the Mie theory, one can determine the EM field at all the points inside the particle and at all points of the homogeneous medium in which the particle is embedded. The mathematical expressions mainly describe how much light is scattered, absorbed, and extinguished by the particle. Mie theory is an analytical solution of Maxwell's equations for the scattering of EM radiation by a particle, and it describes the optical response of a spherical particle. Mie theory requires dielectric constants of the particle and the surrounding medium as input parameters.

Scattering of EM waves through homogeneous, isotropic, and spherical nanoparticles was first modeled by the Mie theory using a multipole expansion approach [59, 65]. This approach offers an analytical solution to the incident and scattered fields. For the theoretical solution, a plane EM wave illumination of a spherical metallic particle (radius, $r = a$) embedded in a medium

with a real refractive index (non-absorbing medium) is considered. The time-harmonic EM field $(\boldsymbol{E}, \boldsymbol{H})$ considered to be a divergence-free, must satisfy Helmholtz' equation, and $\boldsymbol{E}(\boldsymbol{r})$ and $\boldsymbol{H}(\boldsymbol{r})$ are inter-dependent [65]. In spherical coordinates, the general solution of Maxwell equations in a source-free space is given by the spherical vector harmonics $\boldsymbol{M}(\boldsymbol{r})$ and $\boldsymbol{N}(\boldsymbol{r})$. As explained in **Section 1.4.1** (**Chapter 1**), the incident electric field takes the form by using spherical vector harmonics, as represented by Eq. (1.4) (**Chapter 1**)

$$\boldsymbol{E}_i = \sum_{m=0}^{\infty}\sum_{n=m}^{\infty}(B_{emn}\boldsymbol{M}_{emn}^{(1)} + B_{omn}\boldsymbol{M}_{omn}^{(1)} + A_{emn}\boldsymbol{N}_{emn}^{(1)} + A_{omn}\boldsymbol{N}_{omn}^{(1)}) \tag{2.1}$$

The vector spherical harmonics generated by the scalar fields mentioned in Eq. (1.5), and (1.6) (**Chapter 1**), are expressed as

$$\boldsymbol{M}_{emn} = \frac{-m}{sin\theta} sin\, m\phi\, P_n^m(cos\,\theta)\, z_n(\rho)\hat{\boldsymbol{e}}_\theta - cos\, m\phi \frac{dP_n^m(cos\,\theta)}{d\theta}\, z_n(\rho)\hat{\boldsymbol{e}}_\phi,$$

$$\boldsymbol{M}_{omn} = \frac{m}{sin\theta} cos\, m\phi\, P_n^m(cos\,\theta)\, z_n(\rho)\hat{\boldsymbol{e}}_\theta - sin\, m\phi \frac{dP_n^m(cos\,\theta)}{d\theta}\, z_n(\rho)\hat{\boldsymbol{e}}_\phi,$$

$$\boldsymbol{N}_{emn} = \frac{z_n(\rho)}{\rho} cos\, m\phi\, n(n+1)\, P_n^m(cos\,\theta)\, \hat{\boldsymbol{e}}_r + cos\, m\phi \frac{dP_n^m(cos\,\theta)}{d\theta} \frac{1}{\rho}\frac{d}{d\rho}[\rho z_n(\rho)]\hat{\boldsymbol{e}}_\theta -$$

$$m\, sin\, m\phi \frac{P_n^m(cos\,\theta)}{sin\,\theta} \frac{1}{\rho}\frac{d}{d\rho}[\rho z_n(\rho)]\hat{\boldsymbol{e}}_\phi,$$

$$\boldsymbol{N}_{emn} = \frac{z_n(\rho)}{\rho} sin\, m\phi\, n(n+1)\, P_n^m(cos\,\theta)\, \hat{\boldsymbol{e}}_r + sin\, m\phi \frac{dP_n^m(cos\,\theta)}{d\theta} \frac{1}{\rho}\frac{d}{d\rho}[\rho z_n(\rho)]\hat{\boldsymbol{e}}_\theta +$$

$$m\, cos\, m\phi \frac{P_n^m(cos\,\theta)}{sin\,\theta} \frac{1}{\rho}\frac{d}{d\rho}[\rho z_n(\rho)]\hat{\boldsymbol{e}}_\phi, \tag{2.2}$$

Since $sin\, m\phi$ is orthogonal to $cos\, m'\phi$ for all m and m', it follows that $\boldsymbol{M}_{emn}$ and $\boldsymbol{M}_{omn}$ are orthogonal in the sense that

$$\int_0^{2\pi}\int_0^{\pi} \boldsymbol{M}_{em'n'} \cdot \boldsymbol{M}_{omn} \sin\theta\, d\theta\, d\phi = 0 \qquad \text{(all } m, m', n \text{ and } n').$$

Similarly, $(\boldsymbol{N}_{omn}, \boldsymbol{N}_{emn})$, $(\boldsymbol{M}_{omn}, \boldsymbol{N}_{omn})$, and $(\boldsymbol{M}_{emn}, \boldsymbol{N}_{emn})$ are mutually orthogonal sets of functions. As these vector spherical harmonics are orthogonal to each other, and once the electric field is determined, the magnetic field can be calculated by

$$\boldsymbol{H}(\boldsymbol{r}) = -\frac{i}{\omega\mu}\nabla\times\boldsymbol{E}(\boldsymbol{r}), \tag{2.3}$$

where μ is the magnetic permeability of the medium. Using Eq. (1.4) (**Chapter 1**), the magnetic field in the multipole expansion form is written as

$$\boldsymbol{H}_i = \frac{-i}{Z}\sum_{m=0}^{\infty}\sum_{n=m}^{\infty}(A_{emn}\boldsymbol{M}_{emn}^{(1)} + A_{omn}\boldsymbol{M}_{omn}^{(1)} + B_{emn}\boldsymbol{N}_{emn}^{(1)} + B_{omn}\boldsymbol{N}_{omn}^{(1)}) \tag{2.4}$$

where $Z = \frac{1}{\tilde{n}_{medium}}\sqrt{\frac{\mu_0}{\epsilon_0}}$ is the impedence of the surrounding medium, μ_0 and ϵ_0 are the magnetic permeability and electric permittivity in the vacuum. $\tilde{n}_{medium}$ is the refractive index of surrounding medium.

The orthogonality of all the vector spherical harmonics, implies that the expansion coefficients are of the form

$$B_{emn} = \frac{\int_0^{2\pi}\int_0^{\pi}\boldsymbol{E}_i\cdot\boldsymbol{M}_{emn}\sin\theta\, d\theta\, d\phi}{\int_0^{2\pi}\int_0^{\pi}|\boldsymbol{M}_{emn}|^2\sin\theta\, d\theta\, d\phi}, \tag{2.5}$$

With similar expressions for B_{omn}, A_{emn}, and A_{omn}. Depending upon the nature of the incident beam, and orthogonality relations the incident field takes different form. Here, in this thesis, the incident field equation for different beams is discussed in detail in the respective section. Followed by Eq. (1.4) (**Chapter 1**), the general form of a scattered field and internal field are

$$\boldsymbol{E}_s = \sum_{m=0}^{\infty}\sum_{n=m}^{\infty}(b_nB_{emn}\boldsymbol{M}_{emn}^{(3)} + b_nB_{omn}\boldsymbol{M}_{omn}^{(3)} + a_nA_{emn}\boldsymbol{N}_{emn}^{(3)} + a_nA_{emn}\boldsymbol{N}_{omn}^{(3)}) \tag{2.6}$$

$$\boldsymbol{E}_{int} = \sum_{m=0}^{\infty}\sum_{n=m}^{\infty}(c_nB_{emn}\boldsymbol{M}_{emn}^{(1)} + c_nB_{omn}\boldsymbol{M}_{omn}^{(1)} + d_nA_{emn}\boldsymbol{N}_{emn}^{(1)} + d_nA_{omn}\boldsymbol{N}_{omn}^{(1)}) \tag{2.7}$$

a_n, b_n, c_n, and d_n are the unknown coefficients for a given $'n'$, and are obtained from the boundary conditions [65]

$$\boldsymbol{E}_{i,\theta} + \boldsymbol{E}_{s,\theta} = \boldsymbol{E}_{int,\theta}, \qquad \boldsymbol{E}_{i,\phi} + \boldsymbol{E}_{s,\phi} = \boldsymbol{E}_{int,\phi},$$

$$\boldsymbol{H}_{i,\theta} + \boldsymbol{H}_{s,\theta} = \boldsymbol{H}_{int,\theta}, \qquad \boldsymbol{H}_{i,\phi} + \boldsymbol{H}_{s,\phi} = \boldsymbol{H}_{int,\phi}, \qquad (r = a)$$

We are mainly concerned about the incident and scattered field, hence further derivations will be based on the incident and scattered field and their respective coefficients. The permeability of the particle and the surrounding medium are assumed to be the same. In this chapter, we present results on Mie scattering for monometallic (uncoated) and core-shell (coated) nanoparticles. Mie scattering coefficients a_n, and b_n, do not depend on the incident beam profile, and will be the same for different types of incident beams. The scattering coefficients for monometallic and core-shell nanoparticles are determined using formulae given below.

2.1.1 Monometallic nanoparticle

For a monometallic nanoparticle the scattering coefficients depend on the dielectric constant of the metallic nanoparticle, surrounding medium, and radius size are given as [65]

$$a_n = \frac{m_0\psi_n(m_0x)\psi_n'(x) - \psi_n(x)\psi_n'(m_0x)}{m_0\psi_n(m_0x)\chi_n'(x) - \chi_n(x)\psi_n'(m_0x)}, \tag{2.8}$$

$$b_n = \frac{\psi_n(m_0x)\psi_n'(x) - m_0\psi_n(x)\psi_n'(m_0x)}{\psi_n(m_0x)\chi_n'(x) - m_0\chi_n(x)\psi_n'(m_0x)}, \tag{2.9}$$

where $\psi_n(\rho) = \rho j_n(\rho)$ and $\chi_n(\rho) = \rho h_n^{(1)}(\rho)$ are the Riccati-Bessel functions, $\psi_n'(\rho)$ and $\chi_n'(\rho)$ are the respective first order derivatives. $x = ka$ is the size parameter, a is the radius of the metallic nanoparticle. $m_0 = \frac{k_1}{k}$ is the relative refractive index with the respective surrounding medium. $k = \frac{2\pi}{\lambda}\,\tilde{n}_{medium}$, is the wave vector in a surrounding medium and $k_1 = \frac{2\pi}{\lambda}\,\tilde{n}_{particle}$, is the wave vector inside the nanoparticle as presented in Fig. 2.1(a).

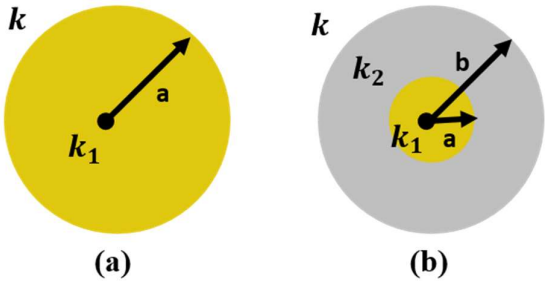

Fig. 2.1 Wave vectors corresponding to (a) monometallic and (b) core-shell nanoparticle.

2.1.2 Core-shell nanoparticles

Similarly, the scattering coefficients for a core-shell nanoparticle depend on size and optical constants or core metal and outer shell metal along with the surrounding medium are given as [65]

$$a_n = \frac{\Psi_n(y)[\Psi_n'(m_2y) - C_n\xi_n'(m_2y)] - m_2\Psi_n'(y)[\Psi_n(m_2y) - C_n\xi_n(m_2y)]}{\chi_n(y)[\Psi_n'(m_2y) - C_n\xi_n'(m_2y)] - m_2\chi_n'(y)[\Psi_n(m_2y) - C_n\xi_n(m_2y)]} \tag{2.10}$$

$$b_n = \frac{m_2\Psi_n(y)[\Psi_n'(m_2y) - D_n\xi_n'(m_2y)] - \Psi_n'(y)[\Psi_n(m_2y) - D_n\xi_n(m_2y)]}{m_2\chi_n(y)[\Psi_n'(m_2y) - D_n\xi_n'(m_2y)] - \chi_n'(y)[\Psi_n(m_2y) - D_n\xi_n(m_2y)]} \tag{2.11}$$

where,

$$C_n = \frac{m_2\Psi_n(m_2x)\Psi_n'(m_1x) - m_1\Psi_n(m_1x)\Psi_n'(m_2x)}{m_2\xi_n(m_2x)\Psi_n'(m_1x) - m_1\Psi_n(m_1x)\xi_n'(m_2x)} \tag{2.12}$$

$$D_n = \frac{m_2\Psi_n(m_1x)\Psi_n'(m_2x) - m_1\Psi_n(m_2x)\Psi_n'(m_1x)}{m_2\Psi_n(m_1x)\xi_n'(m_2x) - m_1\xi_n(m_2x)\Psi_n'(m_1x)} \tag{2.13}$$

where $\xi_n(\rho) = -\rho y_n(\rho)$ is Riccati-Bessel function, $x = ka$, and $y = kb$ are the size parameters, $'a'$ is the inner core radius, and $'b'$ is the overall radius of a coated nanoparticle. Overall radius 'b' represents the total radius a of core and outer shell thickness as shown in Fig. 2.1 (b). $m_1 = k_1/k$, and $m_2 = k_2/k$ are the relative refractive index respective to the

surrounding medium, and $k_1 = \frac{2\pi}{\lambda}\,\tilde{n}_{core}$ is the wave vector inside the core of the nanoparticle, $k_2 = \frac{2\pi}{\lambda}\,\tilde{n}_{shell}$ is the wave vector inside the outer shell coating.

The complex refractive index is written as

$$\tilde{n} = n + ik \tag{2.14}$$

here, n, k are nonnegative, and the dielectric constant $\tilde{\epsilon} = \tilde{n}^2$,

$$\tilde{\epsilon} = \epsilon_1 + i\epsilon_2 \tag{2.15}$$

The dielectric constants of metal are strongly frequency-dependent and contain both real and imaginary components. The real part determines the frequency of the SPP

$$\omega_{sp} = \frac{\omega_p}{\sqrt{\epsilon_1 + 1}}, \tag{2.16}$$

and the imaginary part ϵ_2 of the dielectric function determines the amount of absorption inside the medium [22, 23]. The optical constants of a nanoparticle such as Au and Ag are considered from the data provided by Johnson and Christy [132].

In our study presented in the thesis, the nanoparticle is considered to be kept in different dielectric media such as air ($n_{air} = 1.00$), BK7(glass), and silicon. The BK7 (glass), and silicon show dispersion with changing the wavelength of incident wave. For calculating the refractive index of the dispersive medium BK7 (n_{BK}), and silicon (n_{Si}), the Sellmeier equation is utilized, which is represented as [133, 134]

$$n_{BK}^2\ (\lambda) = 1 + \frac{E_1\lambda^2}{\lambda^2 - F_1^2} + \frac{E_2\lambda^2}{\lambda^2 - F_2^2} + \frac{E_3\lambda^2}{\lambda^2 - F_3^2} \tag{2.17}$$

$$n_{Si}^2(\lambda) = 1 + \frac{G_1\lambda^2}{\lambda^2 - H_1} + \frac{G_2\lambda^2}{\lambda^2 - H_2} + \frac{G_3\lambda^2}{\lambda^2 - H_3} \tag{2.18}$$

where λ is the wavelength of the incident beam, and E, F, G, H are the Sellmeier coefficients determined by a fitting method. Table 2.1 includes the fitting parameters of the Sellmeier equation for dielectric media BK7 (glass), and silicon, and the data are referred from Ref.

Table 2.1. Sellmeier coefficients for BK7 (glass) and Silicon [133, 134]

Material	Sellmeier coefficients					
BK7 (Glass)	E_1	E_2	E_3	F_1	F_2	F_3
	1.0396	$2.3179*10^{-1}$	1.0104	$6.0069*10^{3}$	$2.0017*10^{4}$	$1.0356*10^{8}$
Silicon	G_1	G_2	G_3	H_1	H_2	H_3
	$1.06684293*10^{1}$	$3.04347484*10^{-3}$	1.54133408	$3.01516485*10^{-1}$	1.13475115	$1.10400000*10^{3}$

These three different materials have refractive indices ($n_{air} = 1$, and for dispersive materials $n_{glass} = 1.55\sim1.50$, $n_{silicon} = 3.39\sim2.93$ for wavelength ranging from 300 nm to 900 nm) which are widely separated and therefore cover and fulfill the requirement of being utilized over a wide operating range. Most of the devices largely uses different form of glass, and silicon for their studies. While going from air ($n_{air} = 1$) to a higher refractive index medium such as glass and silicon, the LSPRs responsible for the enhancement in near-field are red-shifted because the resonance condition is satisfied at higher wavelengths [21, 72]. Since LSPR plays a role in the average near-field intensity enhancement, the maximum value of intensity enhancement is termed as LSPR peak wavelength.

2.3 Mie Scattering Algorithm for a Plane Wave

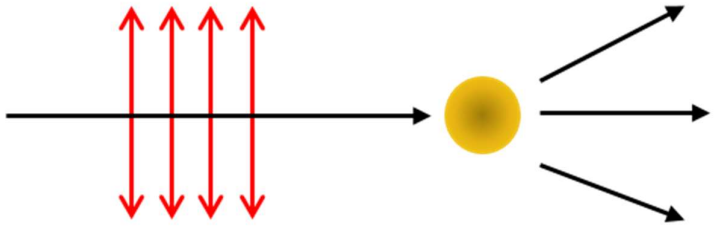

Fig. 2.2 Linearly polarized (red arrows show the orientation of electric field vector) plane wave scattering through a nanoparticle

A linearly polarized incident plane wave with polarization orientation along the x direction illuminating a nanoparticle as shown in Fig. 2.2 is considered and represented in spherical polar coordinates (r, θ, ϕ) as

$$\boldsymbol{E}_i = E_0\, e^{ikrcos\theta}\widehat{e_x}, \tag{2.19}$$

where $\widehat{e_x} = sin\theta cos\phi\widehat{e_r} + cos\theta cos\phi\widehat{e_\theta} - sin\phi\widehat{e_\Phi}$,

E_0 is the amplitude, $k = \frac{2\pi}{\lambda}$ is the wave number, and λ is the wavelength of the incident beam. For a linearly polarized plane wave, $B_{emn} = A_{omn} = 0$ for all m and n, and A_{emn} and B_{omn} survive for $m = 1$ [65]. Substituting these terms into Eq. (2.1), incident EM wave expansion transforms to

$$\boldsymbol{E}_i = \sum_{n=1}^{\infty}(B_{o1n}\boldsymbol{M}_{o1n}^{(1)} + A_{e1n}\boldsymbol{N}_{e1n}^{(1)}), \tag{2.20}$$

The expansion coefficients $B_{o1n}$and A_{e1n} are derived using the orthogonal relations, and for a linearly polarized plane wave $B_{o1n} = -A_{e1n} = A_n$. Thus, the EM field equation for the incident wave is expressed as

$$\boldsymbol{E}_i = \sum_{n=1}^{\infty} A_n(\boldsymbol{N}_{e1n}^{(1)} - i\boldsymbol{M}_{o1n}^{(1)}), \tag{2.21}$$

and the expansion coefficient for *n* multipole order is given as

$$A_n = E_0 i^n \frac{2n+1}{n(n+1)}, \tag{2.22}$$

The incident wave interacts with a spherical plasmonic nanoparticle, and the scattered field is expressed using Eq. (2.6) as

$$\boldsymbol{E}_s = \sum_{n=1}^{\infty} A_n(-a_n \boldsymbol{N}_{e1n}^{(3)} + i b_n \boldsymbol{M}_{o1n}^{(3)}), \tag{2.23}$$

and the superscripts $^{(1)}$ and $^{(3)}$ denote the spherical Bessel function ($j_n(\rho)$) and the spherical Hankel function of the first kind ($h_n^{(1)}(\rho)$) respectively [65].

2.2 Near-field Intensity Enhancement

Using Mie theory, expressions for absorption and scattering cross-sections, angle-dependent scattering functions, and average intensity enhancement in near-field can be derived. Many interesting features of LSPR happen in the near-field, and our discussion is mainly focussed on the "average intensity enhancement" (K_{avg}) in this domain [80]. To study the near-field more precisely, one needs to take into account both the incident and scattered fields as expressed in Eq. (1.9) (**Chapter 1**).The integration in Eq. (1.9) (**Chapter 1**) is done over the surface of the nanoparticle ($r = a$) but could be extended to any distance from the particle [72].

As discussed in **Section 1.5, Chapter 1,** the radial component of the electric field is quite large in the near-field which majorly contributes to the near-field enhancement. Therefore, we discuss the average intensity enhancement. K_{avg} is separated into average radial ($K_{avg,r}$), and average tangential ($K_{avg,t}$) intensity enhancements, and their analytical formulae can be derived using orthogonality properties of the multipoles.

Substituting EM field and expansion coefficient expression from Eqs. (2.21- 2.23) into Eq. (1.9), the average radial (K_r), and tangential (K_t) intensity enhancement for a linearly polarized plane wave is expressed as [72]

$$K_r = \frac{9}{16(\rho)^4}\sum_n \frac{|A_n|^2}{|A_1|^2}\frac{2n^3(n+1)^3}{2n+1}[|a_n|^2|\chi_n|^2 + |\psi_n|^2 - 2\,Re\{a_n\chi_n\}\psi_n]. \quad (2.24)$$

$$K_t = \frac{9}{16(\rho)^4}\sum_n \frac{|A_n|^2}{|A_1|^2}\frac{2n^2(n+1)^2}{2n+1}[|a_n|^2|\chi_n'|^2 + |b_n|^2|\chi_n|^2 + |\psi_n|^2 + |\psi_n'|^2 - 2\,Re\{a_n\chi_n'\}\psi_n' - 2\,Re\{b_n\chi_n\}\psi_n] \quad (2.25)$$

Here, the Riccati-Bessel functions are calculated at the surface of a monometallic nanoparticle ($\rho = ka$) and at the outer surface of the core-shell nanoparticle ($\rho = kb$) [65].

The scattering coefficient a_n, b_n are taken from Eqs. (2.8-2.9), and Eqs. (2.10-2.13) for monometallic and core-shell nanoparticles respectively.

2.4 Results using COMSOL Simulation

We performed a simulation in COMSOL Multiphysics software for an incident linearly polarized plane wave of 400 nm wavelength scattering by an Ag nanoparticle of radius $r = 50\ nm$. The intensity enhancement in the near field of the particle is shown in Fig. 2.3 (a-c) on the x-y, y-z, and x-z planes respectively. Fig. 2.3 (d) shows the far-field view of an Ag nanoparticle.

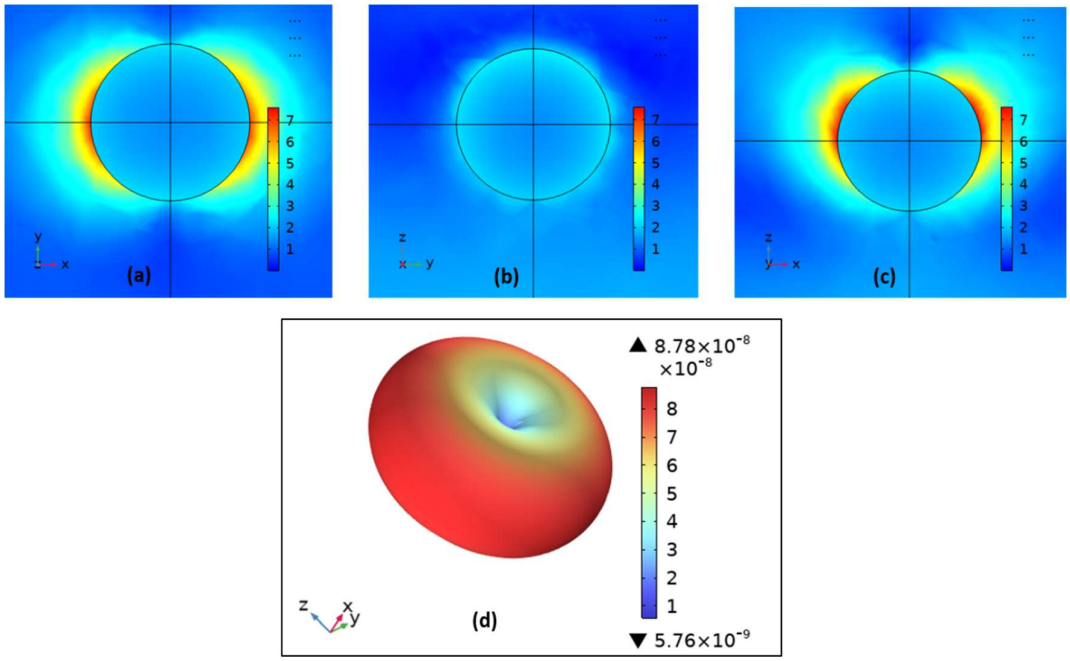

Fig. 2.3 COMSOL Multiphysics Simulation results: Normalized enhanced field (a)x-y axis, (b) y-z axis, (c) x-z axis in the near-field, and (d) far-field view for an Ag nanoparticle of 50 nm radius at $\lambda = 400\ nm$.

Such simulations can be performed for a range of incident beam wavelengths using parametric sweep, whereas obtaining separate components of average intensity enhancement i.e. radial and tangential is not directly possible in COMSOL. We need to extract data from the simulation and plot separately on MATLAB or some other platform, or we need to perform equation-based simulation which is a challenging task.

2.5 Results and Discussion: MATLAB Simulations

To overcome some of these limitations in the COMSOL, we have developed an algorithm on MATLAB platform based on Mie theory for investigating the scattering of a linearly polarized beam from the nanoparticles. The average intensity enhancement for monometallic and core-shell nanoparticles under different conditions is discussed below. For field expansion up to $n = 15$ multipoles are included since higher multipoles do not bring noticeable changes in the results.

2.5.1 Monometallic/Uncoated nanoparticles

The results for Au and Ag nanoparticles having a radius $r = 50$ nm are presented in Fig. 2.4 (a), and (b) respectively in two different dielectric media glass ($n_{glass} = 1.52$) and air ($n_{air} = 1.00$), and these are reproduced results from Mojarad et. al [72]. For these results, a fixed refractive index of a dielectric medium is considered. These results are simulated for a range of wavelengths of the incident beam from 300 nm to 900 nm.

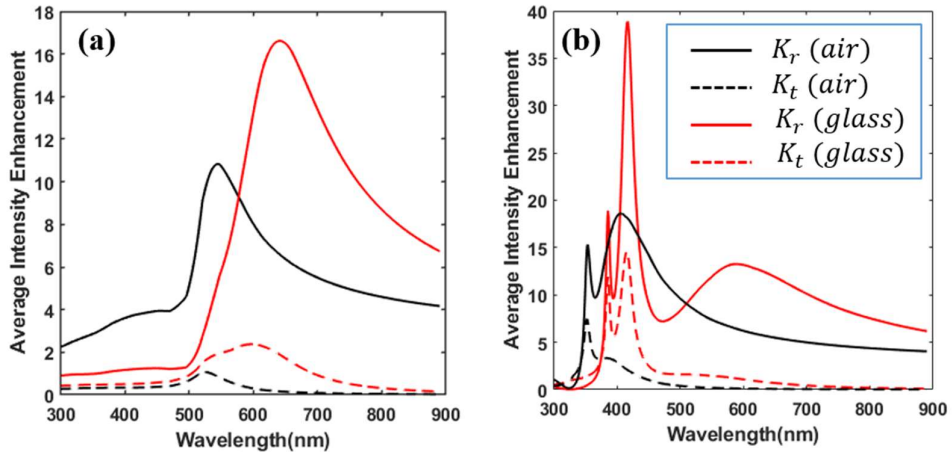

Fig. 2.4 Average radial ($\boldsymbol{K_r}$) and tangential ($\boldsymbol{K_t}$) intensity enhancement for a linearly polarized plane wave scattering from (a) Au, (b) Ag monometallic nanoparticles ($\boldsymbol{r = 50\ nm}$) in dielectric media air, and glass.

It is observed from Fig. 2.4 that the enhancement due to the tangential component is not much significant in comparison to the radial component of near-field intensity. Hence, to examine near-field intensity enhancement, we have mainly observed the radial component of average intensity enhancement (K_r).

Further, we have investigated the interaction of the linearly polarized beam with Au and Ag nanoparticles of varying size of nanoparticle from 1nm to 100nm as presented in Fig. 2.5, and Fig. 2.6. The horizontal axis in the figures represents the range of wavelength of the incident

beam from 300 nm to 900 nm, whereas the vertical axis represents the varying size with a step size of 1nm for both the axes.

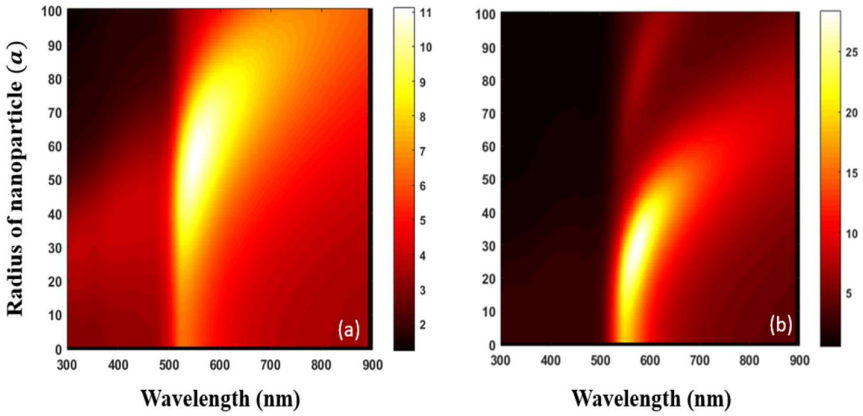

Fig. 2.5 Average radial intensity enhancement (K_r) for an incident plane wave scattering from an Au nanoparticle in dielectric media (a) air, (b) glass.

The average radial intensity enhancement for a linearly polarized plane wave scattered from an Au nanoparticle in the air is shown in Fig. 2.5 (a). Low enhancement is observed for a smaller nanoparticle of radius size less than 40 nm. However, an increase in enhancement is observed as the size of the nanoparticle increases and this is demonstrated in Fig. 2.5 (a). A maximum enhancement is observed for a nanoparticle with a radius in the range of 45 nm-65 nm and this reaches to 11.13 for the Au nanoparticle of size 55 nm at incident wavelength 548 nm in air. Further, a decrease in enhancement is observed on increasing size of nanoparticle and this continues to decrease till 100 nm of radius size. The average radial intensity enhancement for an Au nanoparticle of radius ranging from 1 nm to 100 nm in glass is also investigated and presented in Fig. 2.5 (b). A significant enhancement is observed in a glass, much greater than in the previous case where the dielectric media for the nanoparticle was air. Nanoparticles of radius size 25 nm-35 nm show maximum enhancement and this value reaches 28.38 for the Au nanoparticle with radius size 30 nm at wavelength 576 nm. The observed enhancement is lesser

than the Au nanoparticle in the air for an Au nanoparticle with a radius size larger than 50 nm in a glass.

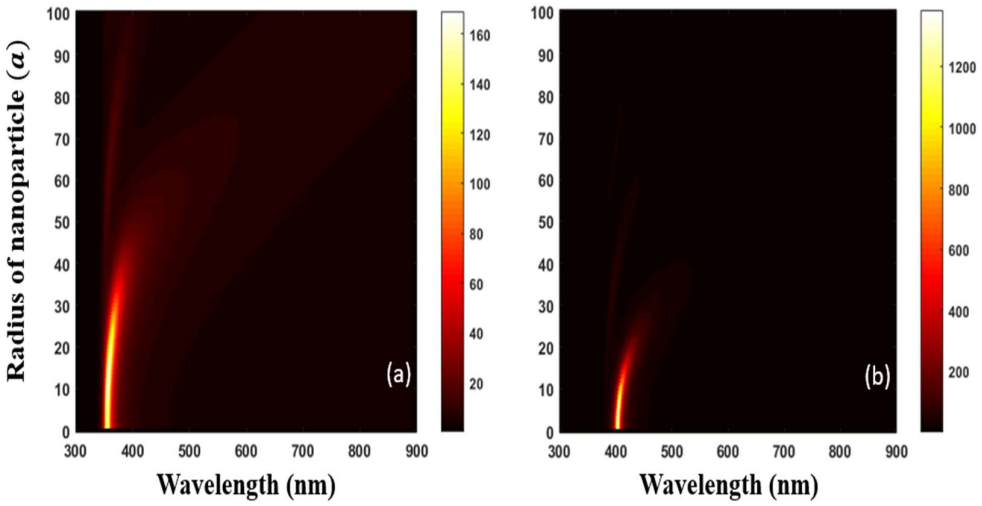

Fig. 2.6 Average radial intensity enhancement (K_r) for an incident plane wave scattering from an Ag nanoparticle in dielectric media (a) air, (b) glass.

Similarly, the average radial intensity enhancements for a linearly polarized plane wave due to an Ag nanoparticle in air and glass are shown in Figs. 2.6 (a), and (b) respectively. In comparison to the results of an Au nanoparticle, significant intensity enhancement was observed for an Ag nanoparticle in Figs. 2.6 (a), and (b) are confined to a narrow wavelength range. Smaller size Ag nanoparticle shows maximum enhancement ranging from 1 nm to 25 nm for a dielectric medium air, and from 1 nm to 10 nm in the case of glass. A maximum enhancement value 169.1 is observed at 357 nm wavelength for 11 nm radius size Ag nanoparticle in air, and this reached to a value 1384 at 404 nm wavelength for 3 nm of radius size Ag nanoparticle in glass. A decrease in enhancement factor is also noted with further increase in the size of Ag nanoparticles as shown in Figs 2.6 (a) and (b). Table 2.2. shows the

maximum enhancement factor observed for Au, Ag nanoparticles in different dielectric media, and the data has been extracted from Fig. 2.5, and Fig. 2.6.

Table 2.2. Maximum Enhancement factor observed for Au and Ag nanoparticles under Plane Wave illumination

Nanoparticles	λ (nm)	Radius (nm)	K_r
Au in air	548	55	11.13
Au in glass	576	30	28.38
Ag in air	357	11	169.10
Ag in glass	404	3	1384

2.5.2 Core-shell nanoparticles

Here, an examination has been carried out to analyze the average radial intensity enhancement due to the plasmonic response of core-shell nanoparticles for an incident plane wave with varying wavelengths ranging from 300 nm to 900 nm. Jana et al. prepared the Ag coated Au hydrosols with particle size varying from 12 nm to 200 nm. The NPs having a 12 nm diameter of Au core and coated with a Ag shell of variable size were prepared using seeding growth method and tested as a substrate for SERS. We adopted the size parameters to examine scattering behaviour [134].

The overall radius of a coated nanoparticle is $b = 20$ nm with core radius $a = 6$ nm radius and outer shell of 14 nm thickness. Interaction of a nanoparticle is considered in three different dielectric media namely air, BK7 (glass), and silicon (Refractive index, **Section 2.1**). Multiple LSPR peaks showing average intensity enhancement are found, depending upon different plasmon modes, geometry of the nanoparticles, and dielectric medium. According to the strength of intensity enhancement we define the LSPR peaks as the first order, second order, and so on.

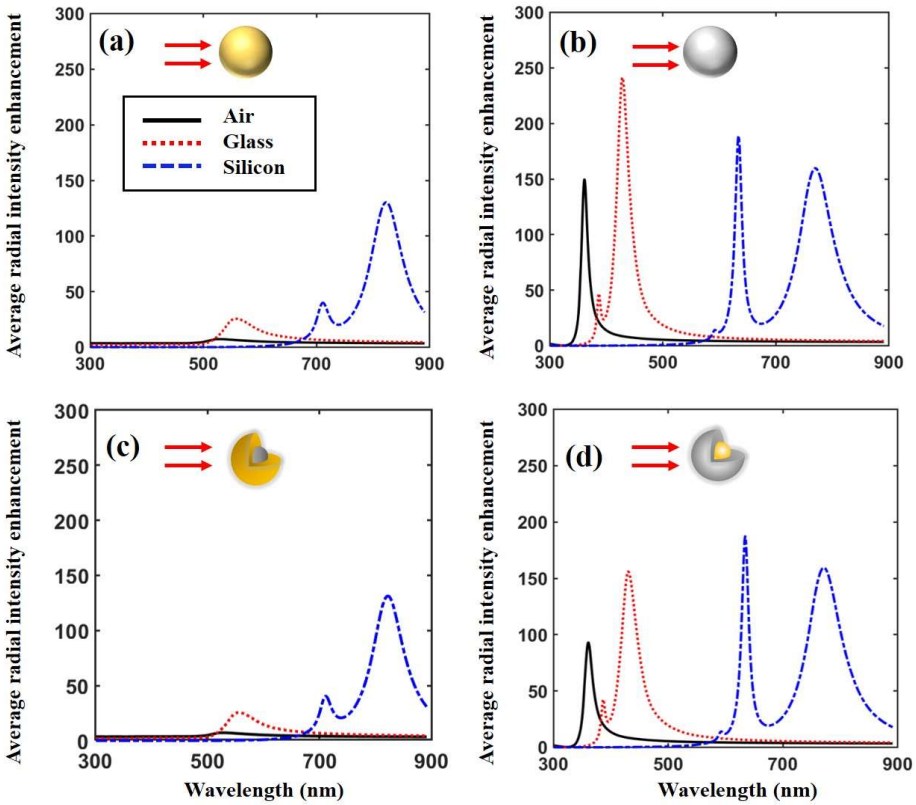

Fig. 2.7 Average radial intensity enhancement in case of an incident linearly polarized PW interacting with (a) an uncoated Au (b) an uncoated Ag, (c) Ag@Au, and (d) Au@Ag nanoparticles in different dielectric media air (black), BK7 (glass) (··· red), and silicon (- – - blue).

Enhancement factors for an uncoated Au and Ag nanoparticle with radii 20 nm, and coated Ag@Au nanoparticle, and Au@Ag nanoparticle having an inner core radius of 6 nm and an overall radius of 20 nm in three different dielectric media are presented in Fig. 2.7 (a)-(d) respectively. A horizontal and vertical axis in Figs. 2.7 represents the wavelength and average radial intensity enhancement, respectively. A single LSPR peak showing enhancement factor of 7.282 for an uncoated Au nanoparticle is observed at wavelength 527 nm in air and this shifts to wavelength 558 nm in BK7 having an increment in enhancement factor to 25.62. Usually, a single LSPR peak is observed for an uncoated Au nanoparticle due to a dipolar resonance but in a silicon medium, two LSPR peaks are observed due to the involvement of quadrupole mode. The first-order LSPR peak at wavelength 823 nm shows an enhancement

factor of 130.4, whereas the second-order LSPR peak shows an enhancement factor of 39.99 at wavelength 711 nm as shown in Fig. 2.7 (a). A single LSPR peak showing an enhancement factor of 149.5 at wavelength 361 nm in air is observed for an uncoated Ag nanoparticle, whereas multiple LSPR peaks are noticed in dielectric media BK7 and silicon as shown in Fig. 2.7(b). The enhancement factor for Ag nanoparticle reaches to 241.3 for the first order LSPR peak at 429 nm wavelength. A second-order LSPR peak appears due to quadrupole mode at wavelength 387 nm showing an enhancement factor of 47.02 in BK7. The first-order LSPR peak for an Ag nanoparticle in silicon medium at wavelength 770 nm shows an enhancement factor of 159.7 and increases to a value of 188.9 for the second-order LSPR peak at wavelength 637 nm.

For an Ag@Au nanoparticle, the enhancement factor is 7.252 at wavelength 525 nm in air and this increases to 25.51 at wavelength 556 nm for BK7 dielectric medium due to the higher index as shown in Fig. 2.7(c). In silicon medium, the intensity enhancement factor reaches 131.3 for a first-order LSPR peak at 822 nm wavelength, whereas the enhancement factor for a second-order LSPR peak reaches 40.34 at 711 nm wavelength. On the other hand, the enhancement factor is 93.13 at wavelength 361 nm for an Au@Ag nanoparticle in air as shown in Fig. 2.7(d). The first order LSPR peak shows the enhancement factor of 156 shifts at wavelength 430 nm in BK7, whereas the second-order LSPR peak appears at the wavelength 387 nm and shows an enhancement factor of 42.4. In silicon medium, the enhancement factor for the first LSPR peak reaches to value 159.4 at wavelength 771 nm, whereas the second order LSPR peak is observed at wavelength 634 nm having 187.3 enhancement factor. Along with two LSPR peaks, a kink is also observed at around 600 nm in silicon medium for an Ag nanoparticle and an Au@Ag core-shell nanoparticle which shows the involvement of higher multipole order as highlighted in Figs. 2.7 (b), and (d).

From the above results it is observed that uncoated Au nanoparticle, and coated Ag@Au nanoparticle show lesser intensity enhancement in comparison to an uncoated Ag nanoparticle, and a coated Au@Ag nanoparticle. It is also observed that a coated Au@Ag nanoparticle is an appropriate and better option for investigating plasmonic properties in comparison to an Ag@Au nanoparticle.

A further study is carried out to examine the variation in average radial intensity enhancement with the thickness of the Ag shell, and the optimal thickness is also determined based on maximum intensity enhancement. We considered the inner core radius $a = 6\ nm$, and overall radius $b = 20\ nm$ for an Au@Ag core-shell nanoparticle, on the other hand, the overall radius is varied from $b = 10\ nm$ to $b = 100\ nm$. The simulation results show the effect of varying outer Ag shell thickness from 4 nm to 94 nm over the fixed on the average radial intensity enhancement. The horizontal axis represents the wavelength ranging from 300 nm to 900 nm, and vertical axis represents the change in overall radius $'b'$ from 10 nm to 100 nm.

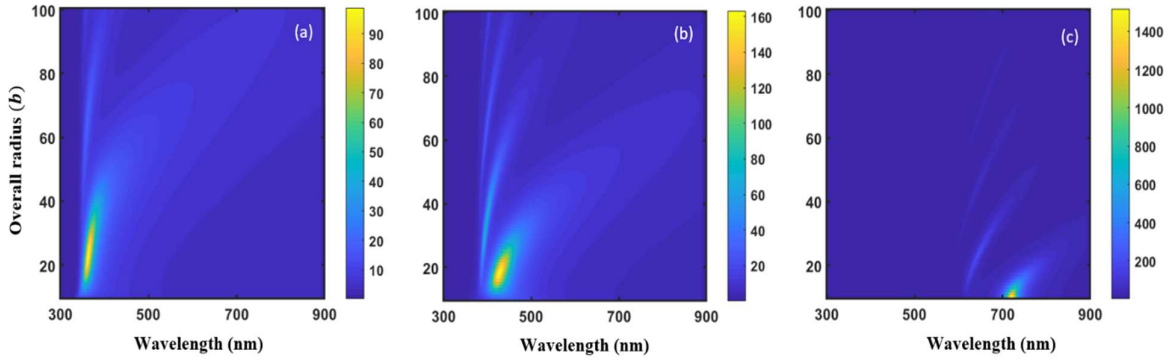

Fig. 2.8 Average radial intensity enhancement for an incident linearly polarized plane wave interacting with an Au@Ag nanoparticle of variable overall radius ranging from 20 nm to 100 nm and in different dielectric media (a) air, (b) BK7 (glass), and (c) silicon.

Results presented in Fig. 2.8 highlight a change in average radial intensity enhancement with varying outer shell thickness. The color bar shows the average radial intensity enhancement.

To further discuss results from Fig. 2.8, the data has been extracted manually and tabulated in Table 2.3.

Table 2.3 Maximum Enhancement factor for a varying Ag shell thickness of an Au@Ag core-shell nanoparticle (Au core radius $a = 6\,nm$) under a Plane Wave illumination

Overall radius, b (nm)	Air	BK7 (glass)	Silicon
40	38.16 (382 nm)	62.84 (403 nm)	58.35 (716 nm)
60	18.34 (358 nm)	25.76 (395 nm)	39.58 (694 nm)
80	14.88 (373 nm)	20.71 (415 nm)	30.86 (682 nm)

In Table 2.3, the maximum enhancement factor is observed for the overall radius of 40 nm, 60 nm, and 80 nm at respective wavelengths. A maximum enhancement factor of 62.84 at wavelength 403 nm is noticed in the BK7 medium.

2.5 Conclusion

In this chapter, we developed a Mie scattering algorithm on the MATLAB platform for a linearly polarized beam interacting with a monometallic or core-shell nanoparticle. In comparison to commercially available tools to study the Mie scattering, our algorithms on the MATLAB platform are more general and capable of incorporating various fundamental features of beam illuminations in the context of the scattering process. A detailed investigation of average radial intensity enhancement in the near-field is presented for a wide range of wavelengths from 300 nm to 900 nm. We studied the plasmonic response of a monometallic Au and Ag nanoparticle with varying radius size from 1 nm to 100 nm, which influences the

near-field intensity enhancement. Plane-wave illuminating a core-shell Ag@Au and Au@Ag nanoparticles of overall radius 20 nm is also discussed, and the corresponding average radial intensity enhancement is investigated. The average radial intensity enhancement for Ag@Au, and Au@Ag core-shell nanoparticles are compared with uncoated Au, and Ag nanoparticles (radius, $r = 20$ nm). The simulation results showing the effect of varying outer Ag shell thickness for a fixed inner Au core of radius $a = 6\,nm$ on the average radial intensity enhancement is examined.